Applications of Nuclear Techniques (CRETE13)
International Journal of Modern Physics: Conference Series
Vol. 27 (2014) 1460153 (9 pages)

DOI: 10.1142/S2010194514601537

APPLICATION OF THE S^{3}M AND MCNPX CODES IN PARTICLE DETECTOR DEVELOPMENT

MÁRIUS PAVLOVIČ*, KATARÍNA SEDLAČKOVÁ†

Faculty of Electrical Engineering and Information Technology,
Slovak University of Technology in Bratislava, Ilkovičova 3, Bratislava, SK-81219, Slovak Republic
**marius.pavlovic@stuba.sk, †katarina.sedlackova@stuba.sk*

ANDREA ŠAGÁTOVÁ

University Centre of Electron Accelerators,
Slovak Medical University, Ku kyselke 497, Trenčín, SK-91106, Slovak Republic
andrea.sagatova1@szu.sk, andrea.sagatova@stuba.sk

IVAN STRAŠÍK

GSI Helmholzzentrum für Schwerionenforschung GmbH, Planckstrasse 1,
Darmstadt, D-64291, Germany
i.strasik@gsi.de

Published 25 February 2014

Semiconductor detectors can be used to detect neutrons if they are covered by a conversion layer. Some neutrons transfer their kinetic energy to hydrogen via elastic nuclear scattering in the conversion layer, and protons are produced as recoils. These protons enter the sensitive volume of the detector and are detected. In the process of detector development, Monte Carlo computer codes are necessary to simulate the detection process. This paper presents the main features of the S^{3}M code (SRIM Supporting Software Modules) and shows its application potential. Examples are given for the neutron detectors with a conversion layer and for CVD (Chemical Vapor Deposition) diamond detectors for beam-condition monitors at the LHC (Large Hadron Collider). Special attention is paid to the S^{3}M statistical modules that can be of interest also for other application areas like beam transport, accelerators, ion therapy, *etc*. The results are generated by MCNPX (Monte Carlo N-Particle eXtended) simulations used to optimize the thickness of the HDPE (high density polyethylene) conversion layer.

Keywords: SRIM; MCNPX; particle detectors; beam transport.

1. Introduction

The Stopping and Range of Ions in Matter, SRIM, is a well-established and widely used Monte Carlo computer code to simulate transport of ions in matter.[1] It can calculate

different quantities and distributions related to interaction of ions with material targets. However, most of these quantities are only defined when the range of ions is shorter than the target thickness. When the range is longer than the target thickness, the ions pass through the target and their parameters like energy (momentum), position and direction of movement are significantly altered by the target material. In this case, SRIM only generates a special record file in the ASCII format. This file needs to be further processed in order to evaluate the influence of the target material on the ion beam and/or to create an input for further calculations. For this purpose, a dedicated S^3M (SRIM Supporting Software Modules) code has been developed.[2] This paper describes its main modules with special emphasis on the built-in statistical tools.

2. The S^3M Code

The present version of the S^3M code consists of three types of modules: a data processing module, four statistical modules and two beam transport modules. The data processing module controls the standard file operations and data handling. In addition to this, it can be used to generate a beam input file[3] to exchange data between different files or even different codes and to save processed files as an input for subsequent simulations.

The four statistical modules have the same design philosophy that is applied to statistical analysis of the energy, momentum, position and angle distributions of ions leaving the target. A special filtering function allows rejecting ions with large deviations from the mean value of the distribution. This particular function will be explained and demonstrated later on. The filtered spectrum can be saved as a new file.

The two beam transport modules link the transport of ions in matter with the transport of ion beams in vacuum. One module converts the ensemble of particles to an ion beam represented by its sigma matrix. The other module performs the transfer matrix transformation of ion coordinates as defined in ion optics. The beam transport module allows calculating the beam transport in complex systems consisting of standard ion-optical elements as well as matter-containing elements like scattering foils, stripping foils, tandem accelerators,[4] range shifters, vacuum windows, air gaps, *etc.* While the action of the standard ion-optical elements is represented by the transfer matrix, the action of the matter-containing elements is treated using Monte Carlo simulations. The S^3M code provides an interface and data conversion between those two approaches.

3. Statistical Tools of the S^3M Code

The statistical tools of the S^3M code can be best explained using a demonstrative example of 5.48 MeV α-particles passing through a 1 mm air gap. This example corresponds to the calibration of a neutron detector with a conversion layer using ^{241}Am. The interaction of the α-particles with air has been simulated in SRIM, and the record file of the transmitted α-particles has been imported to S^3M. SRIM was run with a mono-energetic point-like zero-emittance source of α-particles. The air gap scatters the α-particles and reduces their energy, which is a stochastic process resulting in certain energy

(momentum), position and angle distributions of the transmitted α-particles. These distributions can be displayed, analyzed and processed by the four statistical modules.

3.1. *Basic analysis*

Basic analysis yields the maximum and minimum value in the data record, the total span of the distribution, the mean value and the standard deviation. One standard deviation and three standard deviations are quoted. In addition, the distribution can be plotted in linear or semi-logarithmic scales, and numerical data corresponding to the displayed histograms can be copied to the clipboard. The user can control the histogram resolution.

3.1.1. *The filtering function*

In the process of ion interaction with matter, the majority of ions lose their energy via electronic stopping and undergo small angular deflections due to multiple Coulomb scattering. A few ions undergo elastic nuclear scattering resulting in much higher energy loss and large scattering angles. These ions can be best visible in the semi-logarithmic scale. The large energy loss is accompanied by a large scattering angle that becomes a large position deviation after a drift space. Figure 1 (left panel) shows the energy spectrum of the α-particles after passing the 1 mm air gap and the corresponding cross section of the α-particles following 1 m drift space (right panel) in the real space. The cross section has been obtained using the S³M beam transport module by applying the drift space transfer matrix to the file of the transmitted particles. The transformed file can be saved as a new file and used as an input file for further calculations.

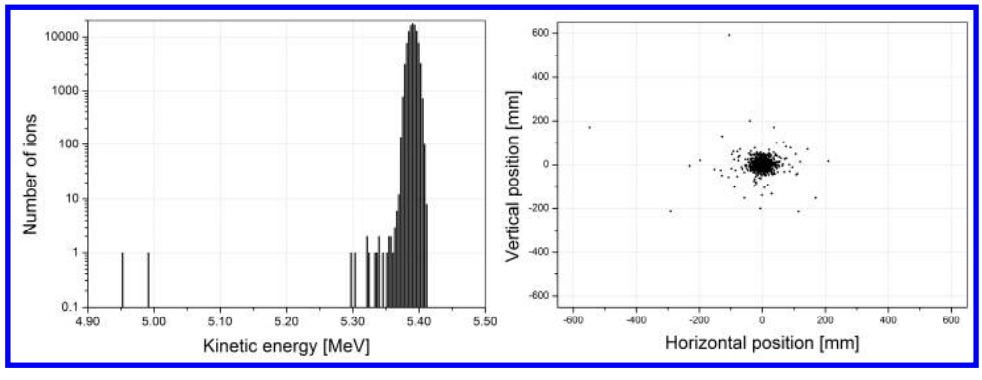

Fig. 1. Energy spectrum of the 5.48 MeV α-particles after passing 1 mm layer of air (left) and the corresponding cross section of the particle distribution in real space following 1 m long drift space (right).

In many situations, especially if the scattered particles are further transported by an ion-optical system, the largely scattered particles are likely to be lost from the beam. There are basically two main reasons for this loss. The particles' energy is "wrong" and the particles get displaced too much in dispersion regions of the beam transport system. In addition to this, the particles' large offset may bring them to the beam pipe wall. In

order to take these effects into account, the filtering function is included in the S^{3}M statistical modules. This function enables the user to set thresholds for particle energy, momentum, angle and/or position. This threshold is specified in multiples of the standard deviation of the corresponding distribution. The cutoff rejects the particles from statistical analysis but keeps them in the original file, hence the cutoffs can be interactively adjusted by the user. Nevertheless, the filtered file can be saved as a new file and used for further calculations while keeping the lost particles in the original file. The filtering function, when applied to the position distributions, can be effectively used to simulate collimators in the beam line.[3]

3.2. *The sigma-matrix routine*

The sigma matrix routine displays the particle distribution in real space and two phase spaces (horizontal and vertical) and calculates the four-dimensional sigma matrix using its statistical definition.[2] This routine is particularly relevant for beam transport calculations using dedicated ion-optical codes like TRANSPORT, WinAGILE, *etc.* based on the matrix formalism. The sigma matrix (or the corresponding Twiss parameters) is expected by these codes as an input. In this way, the Monte Carlo simulations of the beam transport through a matter-containing element can be followed by beam transport calculations in ion-optical elements following the matter-containing one. These beam transport calculations can be done either using an external code or the built in S^{3}M beam transport module that allows entering the transfer matrix. It is, however, not equipped with specialized ion-optical tools like matching ion-optical constraints, displaying beam envelopes, *etc*.

In the context of the sigma matrix routine, the filtering function is quite an important tool keeping the emittance diagrams obtained from Monte Carlo simulations close enough to the assumed elliptical model. Individual particles with large offsets from the center of the emittance diagram do not fit to this elliptical model and — if included into the statistical evaluation of the emittance diagram — increase virtually the beam emittance. Because they are likely to be lost during the beam transport, they should better be filtered out from the particle set.

4. Application Examples of the S^{3}M Code in Development of Particle Detectors

4.1. *Neutron detectors with a conversion layer*

Semiconductor detectors can be used to detect neutrons if they are covered by a proper conversion layer. In the conversion layer, some neutrons transfer their kinetic energy to hydrogen via elastic nuclear scattering, and protons are produced as recoils. These protons enter the sensitive volume of the detector and are detected. The working principle of a neutron detector with a HDPE (high density polyethylene) conversion layer is shown schematically in Fig. 2.

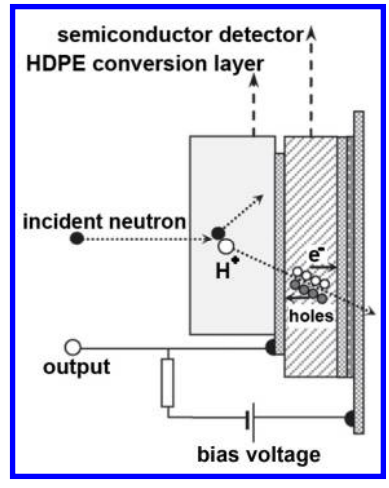

Fig. 2. Working principle of a semiconductor neutron detector with a HDPE conversion layer.

Semiconductor neutron detectors belong to very promising types of neutron detectors. They are typically small, compact and, as such, well-suited for various applications like neutron imaging,[5] high-speed tomography[6] or neutron resonance imaging.[7] Neutron imaging can serve as a complementary method to X-ray radiography. X-ray radiography is unable to achieve a good contrast for light element imaging, and the X-rays can hardly penetrate materials with mass number higher than 90. Neutron imaging has a potential to overcome these drawbacks. Recent results show that position-sensitive semiconductor detectors with conversion layers or reactive films reach better properties than CCD-cameras routinely used in neutron digital imaging technologies, particularly in terms of spatial resolution, linearity and dynamic range.[5] Investigated semiconductor neutron detectors are usually based on silicon,[5] but alternative materials like GaAs[8] or CdTe[9] can also be used. High radiation hardness of bulk semi-insulating GaAs against high energy photons and neutrons predestines this material to be a prospective candidate for neutron detectors.

4.1.1. *Detector testing with a calibration source*

For testing and calibration purposes, a GaAs detector was irradiated first without the conversion layer with α-particles emitted from an ^{241}Am radioactive source. The advantage of such testing is that the energy of the incoming radiation is well defined. The source emits α-particles at two discrete energies: 5.480 MeV (yield 84.5%) and 5.437 MeV (yield 13%). Technically, it was not possible to put the source in direct contact with the detector. Therefore, it was put in front of the detector separated from the conversion layer by a 1 mm air-gap. Transport of the α-particles through the air-gap changes their energy spectrum, which was simulated using SRIM and evaluated using S³M. Figure 3 shows the energy spectrum of α-radiation at the detector surface (left panel) and the measured detector response (right panel).

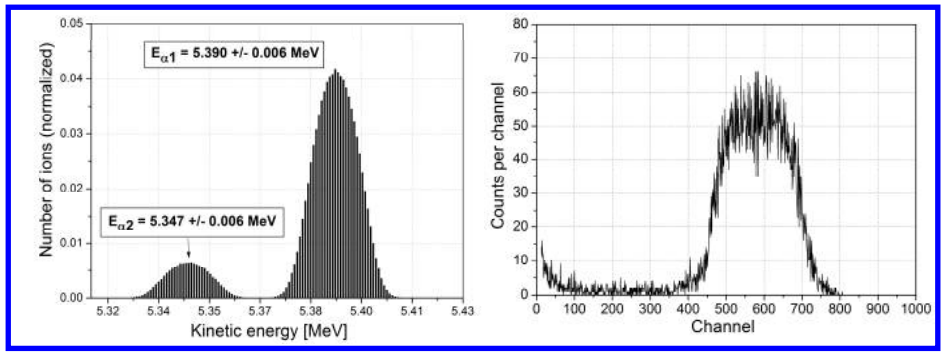

Fig. 3. Energy spectrum of the ^{241}Am α-radiation at the detector surface (left) and the measured detector response at bias voltage 100 V (right).

Unlike the photon radiation, there is no "photo-peak" in the detector response because the interaction of charged particles with matter is a continuous slowing-down process. The situation becomes even more complicated in the case of incident neutron radiation. Even a mono-energetic source of neutrons would generate a complex energy spectrum of proton recoils at the exit of the conversion layer. In order to optimize the detector design under realistic conditions, MCNPX simulations were performed.[10]

4.1.2. *MCNPX simulations*

One of the main purposes of the MCNPX simulations was optimization of the conversion layer thickness. It is obvious that a thicker conversion layer produces more protons, but at the same time, if it is thicker than the range of the recoil protons, a certain amount of them will stop in the conversion layer without reaching the detector. That is why an optimal thickness is expected. A model used in the simulations comprised a point-like ^{239}Pu–Be neutron source collimated into a cone and a HDPE conversion layer. The source-to-detector distance was 10 mm, and the thicknesses of the conversion layer varied from 50 to 1500 μm. The assumed differential flux density of the source is depicted in Fig. 4 (left panel). The mean energy of the neutrons is about 4.3 MeV. The

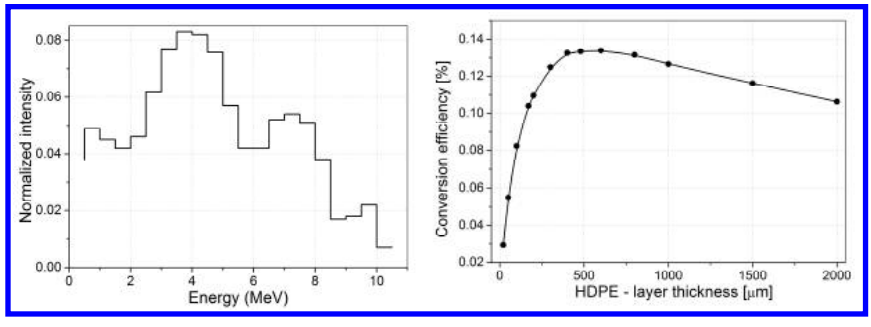

Fig. 4. Assumed neutron spectrum of the ^{239}Pu–Be source used in the MCNPX simulations (left) and conversion efficiency as a function of the HDPE thickness (right).

flux density of protons at the exit of the conversion layer was simulated in order to determine the conversion efficiency (the conversion efficiency is defined as the ratio between the integral proton flux density at the exit of the conversion layer to the neutron flux density on its top side). The conversion efficiency is consistent with detection efficiency under the assumption that all charged particles entering the detector are registered. The conversion efficiency as a function of the conversion layer thickness is shown in Fig. 4 (right panel). The maximum conversion efficiency (0.135%) was found at 500 μm HDPE conversion layer thickness.

4.2. *Development of the CVD diamond beam-condition monitors*

The other applications of the S³M code concerned simulations of the energy deposition in CVD (chemical vapor deposition) diamond detectors developed for the LHC (Large Hadron Collider) BCMs (beam-condition monitors).[11,12] The BCM setup used in our simulations consisted of five detectors, whereby each detector consisted of nine layers (see Fig. 5).

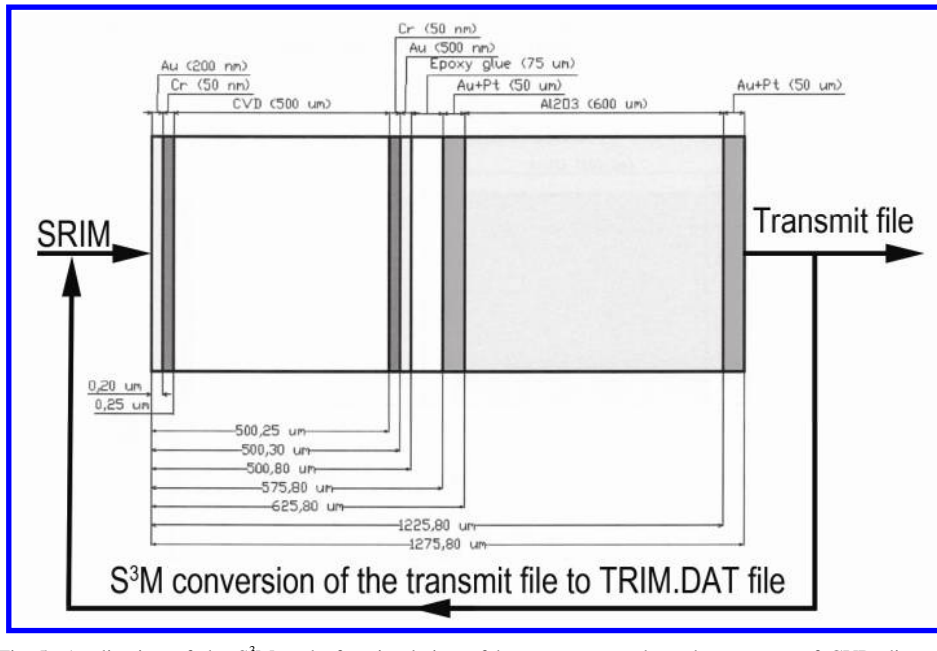

Fig. 5. Application of the S³M code for simulation of beam transport through a system of CVD diamond detectors used as beam-condition monitors at LHC.

The simulations were conveniently done using SRIM and S³M in a step-wise manner. The beam transport through a single detector unit was simulated in SRIM, and the file of transmitted ions was recorded. S³M enables converting this file into the TRIM.DAT input file that can be used for a subsequent SRIM run for the next detector unit. This detector unit has the same configuration as the previous one, but it is now entered by particles

with modified energy spectrum. As an example, the energy of an originally mono-energetic 100 MeV proton beam is reduced to 96.57±0.24 MeV, 93.04±0.34 MeV, 89.41±0.44 MeV, 85.67±0.55 MeV and 81.80±0.60 MeV after passing the first, second, third, fourth and fifth detector units, respectively. The energy straggling values represent one standard deviation of the corresponding energy spectrum. The data were obtained by statistical analysis of the TRANSMIT.TXT files generated by SRIM and converted to the TRIM.DAT files by S^3M. In this way, it was possible to investigate systematically the detector setup in a wide energy range of incident protons and to get more accurate information about the energy deposition in individual detector units. Information about the energy deposition in the CVD volume could be resolved from the IONIZ.TXT files.

5. Discussion and Conclusions

This paper reviewed the statistical tools implemented in the S^3M code and showed some of their possible applications. Among a broad spectrum of possible applications, the main attention was paid to development of modern particle detectors, namely neutron detectors with a conversion layer and CVD diamond detectors for beam-condition monitors. The S^3M code broadens considerably the application potential of the SRIM code and enables obtaining additional information that is not directly provided by SRIM. Combination of SRIM and S^3M speeds up SRIM simulations in complex multi-layered structures. Together with the beam transport module, it can be used to simulate beam transport through combined ion-optical and matter-containing systems.

The MCNPX code has been used for design and optimization of the neutron semiconductor detectors with a HDPE layer. This code can be applied to more complex problems or particles that are not included in SRIM. However, supporting information like ion range, range straggling, energy loss and energy deposition, *etc.* is frequently needed and can be provided in a convenient and fast way by SRIM and/or S^3M.

Acknowledgments

This work was supported by the Slovak Research and Development Agency under contract No. APVV–0321–11 and by the Scientific Grant Agency under contract No. VEGA–2/0062/13.

References

1. J. F. Ziegler, M. D. Ziegler and J. P. Biersack, *Nucl. Instr. Meth. Phys. Res. B* **268**, 1818 (2010).
2. M. Pavlovič and I. Strašík, *Nucl. Instr. Meth. Phys. Res. B* **257**, 601 (2007).
3. M. Pavlovič and I. Strašík, *Radiation Effects and Defects in Solids* **7–8**, 470 (2009).
4. J. M. Gómez-Guzmán, I. Gómez-Morilla, S. M. Enamorado-Báez, A. I. Moreno Suárez *et al*., *Nucl. Instr. Meth. Phys. Res. B* **281**, 30 (2012).
5. J. Jakubek, C. Granja, T. Holy, E. Lehmann *et al*., *Nucl. Instr. Meth. Phys. Res. A* **569**, 205 (2006).
6. M. Kureta and H. Likura, *Nucl. Instr. Meth. Phys. Res. A* **605**, 81 (2009).

7. T. Kai, M. Segawa, M. Ooi, E. Hashimoto *et al*., *Nucl. Instr. Meth. Phys. Res. A* **651**, 126 (2011).
8. A. Šagátová–Perďochová, M. Ladzianský and V. Nečas, *Nucl. Instr. Meth. Phys. Res. A* **591**, 98 (2008).
9. A. Miyake, T. Nishioka, S. Singh, H. Morii *et al*., *Nucl. Instr. Meth. Phys. Res. A* **677**, 41 (2012).
10. K. Sedlačková, B. Zaťko, A. Šagátová–Perďochová and V. Nečas, *Nucl. Instr. Meth. Phys. Res. A* **709**, 63 (2013).
11. A. Gorišek, V. Cindro, I. Dolenc, H. Frais-Kölbl *et al.*, *Nucl. Instr. Meth. Phys. Res. A* **572**, 67 (2007).
12. V. Cindro, D. Dobos, I. Dolenc, H. Frais-Kölbl *et al*., *J. Instrumentation* **3**(2), P02004 (2008).